

Hydrothermal Coating of the Biodegradable Mg-2Ag Alloy

Meysam Mohammadi-Zerankeshi, Mohammad Zohrevand and Reza Alizadeh * 

Department of Materials Science and Engineering, Sharif University of Technology, Tehran 11365-9466, Iran; meysam.mohammadi@student.sharif.edu (M.M.-Z.); mohammad.zohrevand@student.sharif.edu (M.Z.)

* Correspondence: r.alizadeh@sharif.edu; Tel.: +98-2166165265

Abstract: Developing antibacterial biodegradable Mg alloys is of paramount importance to prevent infection and inflammation during the healing process. In this regard, the Mg-2Ag alloy is proposed as a suitable candidate with appropriate biocompatibility as well as antibacterial activity. However, its rapid degradation rate limits its clinical application. To tackle this problem, the hydrothermal coating technique was employed to synthesize a barrier coating to enhance the degradability of the Mg-2Ag alloy using distilled water as the reagent. Field emission scanning electron microscopy (FESEM) micrographs and X-ray diffraction (XRD) patterns showed that a hydroxide coating was formed on the studied samples. Furthermore, it was observed that the substrate microstructure plays an essential role in the obtained coating quality and hence, the degradation behavior. The dendritic microstructure with the nonuniform distribution of Ag-rich precipitates of the as-cast Mg-2Ag alloy lead to undesirable cracks and holes in the coating owing to Mg deficiency to form $Mg(OH)_2$, whereas the solution-treated alloy with a homogenized microstructure resulted in the formation of a more compact, thick, and integrated coating, which remarkably improved the corrosion resistance of the alloy.

Keywords: antibacterial implant; biomaterial; coating; heat treatment; hydrothermal; Mg-Ag alloy



Citation: Mohammadi-Zerankeshi, M.; Zohrevand, M.; Alizadeh, R. Hydrothermal Coating of the Biodegradable Mg-2Ag Alloy. *Metals* **2023**, *13*, 1260. <https://doi.org/10.3390/met13071260>

Academic Editor: Changdong Gu

Received: 31 May 2023

Revised: 2 July 2023

Accepted: 10 July 2023

Published: 13 July 2023



Copyright: © 2023 by the authors. Licensee MDPI, Basel, Switzerland. This article is an open access article distributed under the terms and conditions of the Creative Commons Attribution (CC BY) license (<https://creativecommons.org/licenses/by/4.0/>).

1. Introduction

The overall longevity and aging of the world's population necessitate the development of new biomaterials with improved properties to treat damaged tissues [1]. Inert materials like Al_2O_3 and bioactive materials such as hydroxyapatite are the first and second generations of biomaterials, which require a second surgery for their removal. However, the third and newest generation of biomaterials is the biodegradable material which can act as a temporary structure to facilitate the tissue-healing process. They allow the adjacent tissue to integrate and proliferate with them, where they will gradually be degraded in a physiological environment and finally, be replaced by the host tissue [2].

Biodegradable Mg-based alloys offer outstanding advantages compared to other alloys, traditionally used to make nondegradable implants, making them revolutionary degradable implants [3,4]. Magnesium alloys have lately gained prominence as raw materials for implants in osteosynthesis and cardiovascular surgeries, where they can be employed as wound-closing devices and also in laryngeal microsurgery [5–9]. Their close density and elastic modulus to human bones allow them to efficiently avoid the stress-shielding effect. In addition, Mg is one of the main elements that play an important role in biological functions [8]. Degradability of magnesium alloys can itself be their main drawback, if not controlled correctly. An accelerated corrosion rate in aqueous environments, followed by the loss of mechanical integrity, would eventually cause implantation failures [1,10]. In addition, the formation of large quantities of hydrogen gas bubbles is another issue in Mg rapid degradation, which may occur mainly in the early weeks after implantation. This may result in an infection or local inflammation [11,12]. Therefore, the degradation behavior of magnesium alloys used as implants should be tailored to match the bone-healing rate. Moreover, implants with antimicrobial properties are highly desirable to

avoid inflammation and infection after surgery. Mg antibacterial activity is insufficient to effectively prevent biofilm formation, which can also lead to implantation failure by keeping cells away from the implant [13].

To tackle these challenges and improve the corrosion resistance as well as antibacterial properties of Mg alloys, different strategies have been employed such as alloying, heat treatment, thermomechanical processing, directional solidification, and coating [14–17]. Among the alloying elements, Ag is known to possess a dynamic antibacterial capability at a relatively low concentration; hence, Mg-Ag alloys have attracted wide attention [7,13,18]. In an investigation [19], the viability of bacteria on solution-treated Mg-6Ag and Mg-8Ag discs was 18.64% and 14.75%, respectively, which is significantly lower than that on pure Mg (more than 50%). Also, Ag has been shown to have positive effects on improving the mechanical properties of Mg. In this regard, it has been reported that the addition of Ag can improve the hardness, strength, and ductility of pure Mg by the incorporation of Ag-containing precipitates and also grain refinement [20,21]. However, Ag addition might negatively affect the corrosion resistance of Mg, as a result of the formation of secondary phases that can act as the cathode in the magnesium matrix and thus play a significant role in microgalvanic corrosion [22]. In this regard, it has been reported [1] that solution heat treatment can significantly lower, or even eliminate, the microgalvanic corrosion due to the dissolution of secondary phases. Indeed, this heat treatment results in the uniform distribution of alloying elements, which itself helps to improve the quality of the corrosion protective film due to the obtained microstructural homogeneity. Moreover, the mechanical strength of the solution-treated alloy would be balanced to some extent as a result of the achieved solution strengthening [1,23]. In this regard, it has been reported [24] that solution heat treatment slightly improves the mechanical strength and markedly decreases the degradation rate of the as-cast Mg-4Ag alloy, owing to the dissolution of the dendritic structure and some of the precipitates.

Previous works indicate that in order to use biodegradable implants in clinical applications, in addition to choosing the appropriate alloy and processing techniques, surface modification is ultimately required [25]. An anticorrosion coating on the surface can inhibit the transmission of corrosive media to the substrate and significantly enhance the corrosion resistance [26,27]. In this regard, different coating techniques such as vapor deposition coating [28], plasma spraying coating [29], organic-based coating [30], and anodic oxide coating [31] have been employed. Also, recent studies have explored the possibility of addressing such issues by surface chemical treatment and the in situ self-assembly of some biocompatible elements such as Mg²⁺-incorporated epigallocatechin gallate (EGCG) [32], 16-Phosphonohexadecanoic acid (16-Pho) [33], and chitosan-functionalized graphene oxide (GOCS) [34]. However, such methods can be considered to be complicated approaches in terms of either equipment or operation for coating Mg alloys. The hydrothermal technique has been identified as one of the most effective and simple approaches for synthesizing an anticorrosion coating on Mg alloys' surface [35]. This method offers remarkable advantages such as a low cost, simplicity, being environmentally friendly, and fast compared to other coating methods [36]. Moreover, the hydrothermal technique can be used to coat relatively large specimens, and can also be commercially scaled up owing to the occurrence of hydrothermal crystallization on a three-dimensional structure [37]. Recently, some publications have outlined the unique corrosion-inhibition properties of coatings produced by the hydrothermal method on some Mg alloys [37–42]. For example, Song et al. [36] synthesized a dual-layer structured corrosion-resistant coating which was composed of Mg(OH)₂ and LiOH on an Mg-9Li alloy by the optimization of the hydrothermal reaction in deionized water. The amount of hydrogen evolved in the coated sample decreased more than 1.5 times at the optimum conditions.

Accordingly, the present investigation proposes a hydrothermal method using deionized water as a precursor solution to create a corrosion-resistant coating on an Mg-2 wt% Ag alloy, as an appropriate antibacterial alloy which has shown adequate antibacterial performance to prevent biofilm formation [15,43]. Also, the effects of solution heat treatment

on the quality of the coating as well as the degradability of this alloy were thoroughly studied.

2. Materials and Methods

2.1. Material Preparation

The Mg-2 wt% Ag alloy (all compositions are in weight percent, hereafter, unless mentioned) was prepared by melting pure Mg (99.99%) and Ag (99.96%) in a graphite crucible utilizing an induction furnace under the protection of the covering flux (MAGREX 60, Vesuvius plc, London, United Kingdom). After melting the Mg at 750 °C, Ag was added to achieve the desired composition, followed by holding the melt for 10 min at this temperature and mechanical stirring by a stainless-steel rod for 5 min. Then, it was poured into a preheated (210 °C) steel mold. To evaluate the validity of chemical composition after casting, the atomic absorption spectroscopy (AAS) technique was carried out. The solution treatment was performed at 400 °C for 16 h in an electrical furnace. Hereafter, the as-cast and solution-treated samples are named AC and ST, respectively.

2.2. Hydrothermal Coating

Prior to the hydrothermal coating process, the 10 mm × 10 mm × 10 mm samples, both in the AC and ST states, were prepared by grinding with SiC paper up to 1200 grit, and then ultrasonically cleaned in ethanol for 12 min, followed by natural drying in air. The prepared samples were immersed into a stainless-steel Teflon-lined autoclave filled up to 70% capacity with distilled water as the reactor and reagent, respectively. The sample-contained reactor was maintained at 160 °C for 6 h, inside an electrical resistance furnace, and then, after cooling, the coated sample was taken out from the reactor and washed slowly with distilled water and dried with hot air.

2.3. Microstructure Characterization

X-ray diffraction (XRD) analysis (X'Pert Pro MPD, Panalytical, Almelo, The Netherlands) of the uncoated and coated alloys was performed by exposing the surface of the polished samples to Cu-K α radiation ($\lambda = 0.15418$ nm) in the 2θ range of 15–85°. The samples were scanned with an accelerating voltage and scan rate of 40 kV and 2°/min, respectively. In addition, the microstructure of the samples, both the substrate and coating, was studied using field emission scanning electron microscopy (FESEM, MIRA 3 LMU, TESCAN, Brno, Czech Republic), equipped with energy dispersive spectroscopy (EDS). For microstructural characterization of the substrate, after normal grinding and polishing operations, chemical etching was used to reveal the microstructure of the uncoated AC and ST alloys, utilizing nital (92 mL ethanol + 8 mL nitric acid) and picral (6 mL ethanol + 2.5 mL acetic acid + 0.4 gr picric acid + 2 mL distilled water) solutions, respectively.

2.4. Corrosion Tests

Short-term and long-term corrosion behavior of the uncoated and coated alloys was assessed by employing polarization and hydrogen evolution tests, respectively. The phosphate buffer saline (PBS) solution was selected as the simulated body fluid for all corrosion tests, while its chemical composition is given in Table 1. For the electrochemical tests, an Autolab potentiostat/galvanostat instrument and a three-electrode cell setup containing the specimen, Ag/AgCl, and platinum as the working, reference, and counter electrodes, respectively, were utilized. For this purpose, the applied potential range (versus Ag/AgCl electrode) and scan rate were 300 to 300 mV and 5 mV/s, respectively. The corrosion current density (i_{corr}) and corrosion potential (E_{corr}) values were determined using Tafel extrapolation.

Table 1. Chemical composition of the used PBS solution.

| Solution | Chemical Composition (g/L) | | | |
|----------|----------------------------|------|----------------------------------|---------------------------------|
| | NaCl | KCl | Na ₂ HPO ₄ | KH ₂ PO ₄ |
| PBS | 8.00 | 1.15 | 0.20 | 0.20 |

The long-term degradation behavior of the studied materials was studied over 11 days by measuring the volume of the evolved hydrogen from the immersed samples in the PBS solution at 37 ± 0.5 °C. Details of this test, as well as a schematic representation of the used setup, are given elsewhere [15] and only briefly described here. For this test, samples with approximate dimensions of 10 mm × 10 mm were first cold-mounted and then ground up to 2500 grit using SiC paper, in the case of the uncoated ones. To ensure the reproducibility and validity of data, hydrogen evolution tests were performed three times for each material. Also, the surface morphology of the corroded samples was studied by FESEM.

3. Results and Discussion

3.1. Microstructure Evolution

3.1.1. Substrate

The results of the AAS analysis showed that the concentration of Ag is 1.98%, which is very close to the nominal composition. Figure 1 shows the FESEM micrographs of the Mg-2Ag alloy in both the AC and ST states. As can be observed, the as-cast material exhibits a dendritic structure with a nonuniform distribution of Ag-rich precipitates, which are relatively large in size. The EDS map-scan result obtained from the region containing one of this precipitate (region A in Figure 1a) is shown in Figure 1c, where it can clearly be observed that these white particles are Ag-rich precipitates. Similar microstructures have previously been reported in Ag-containing as-cast Mg alloys [24], where the Ag content is usually higher than 1%. For better identification of the phases, XRD was performed on the as-cast alloy and the associated pattern is presented in Figure 2. Accordingly, in addition to α -Mg peaks, some peaks related to the Mg₅₄Ag₁₇ secondary phase could be detected in the pattern, which indicates that the mentioned Ag-rich precipitates in the microstructure of the as-cast material are the Mg₅₄Ag₁₇ phase. On the other hand, as Figure 1b shows, the solution-treated Mg-2Ag alloy possesses a homogenous microstructure with approximately no observable precipitates. It can be deduced that heat treatment at 400 °C for 16 h can significantly decrease the volume fraction of the secondary phases and form a supersaturated solid solution in the Mg-2Ag alloy.

3.1.2. Coating

The XRD pattern of the coated as-cast Mg-2Ag alloy shown in Figure 2 demonstrates the fact that the main constituent of the hydrothermally formed coating is Mg(OH)₂. This is in accordance with previous works [14,36], where the Mg(OH)₂ hydroxide layer was formed on Mg-4Zn and Mg-9Li alloys after hydrothermal coating using deionized water.

The FESEM micrographs of the Mg-2Ag alloy in the AC and ST conditions are depicted in Figure 3. It can be observed that the morphology of the formed magnesium hydroxide is the commonly known hexagonal flake structure units [35,44]. Also, some small irregular-shaped plates with a diameter of 50–70 nm (Figure 3f) as well as flower-shaped clusters with different sizes (Figure 3e) can be observed. Such different Mg(OH)₂ coating morphologies was reported in an Mg-3Al-1Zn (AZ31) alloy hydrothermally synthesized in the temperature and time ranges of 120–160 °C and 1–3 h [44]. Also, the formation of the Mg(OH)₂ coating with flower-shaped clusters distributed in different coating regions was observed in a biodegradable Mg-2Zn-Mn-Ca-Ce alloy [37]. With careful examination of the FESEM micrographs, it can be observed that while the as-cast Mg-2Ag alloy exhibited some microdefects like pores and cracks, the solution-treated one possessed a more uniform and compact coating.

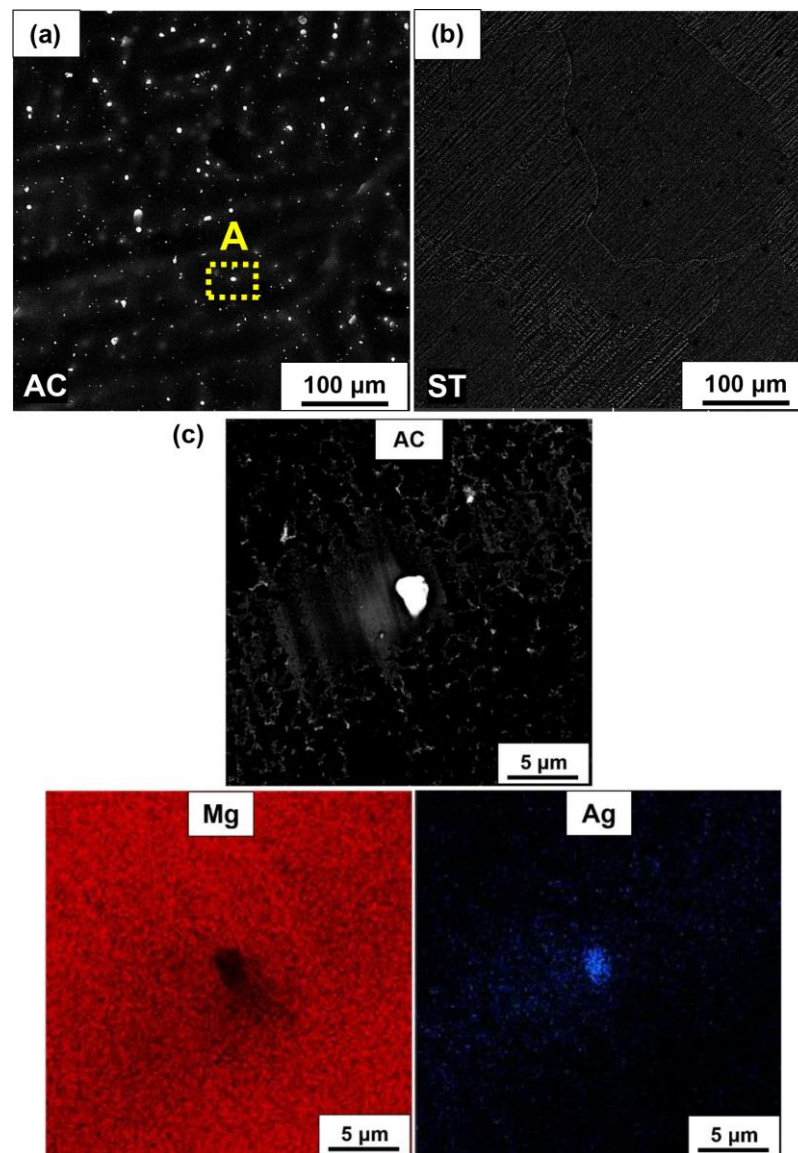


Figure 1. FESEM micrographs of the Mg-2Ag alloy in the AC (a) and ST (b) states. Higher magnification of region A in (a) is represented in (c), together with the corresponding EDS map-scan results.

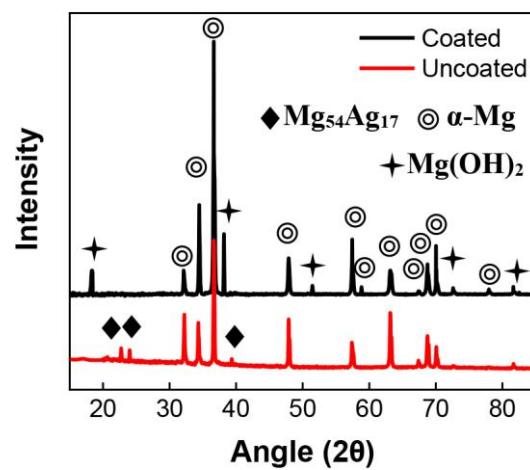


Figure 2. XRD patterns of coated and uncoated Mg-2Ag alloy in the as-cast condition.

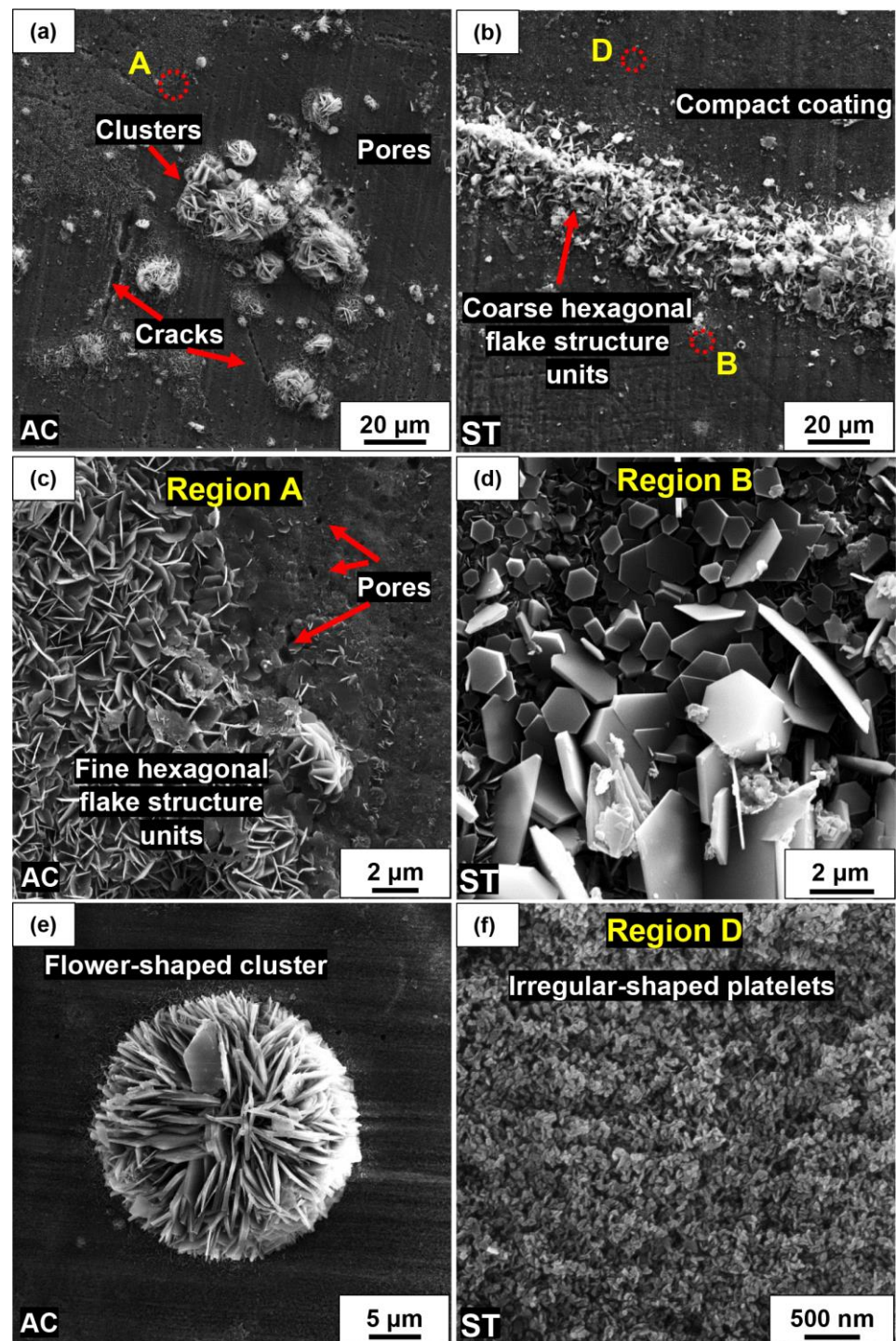


Figure 3. SEM micrographs of the coated Mg-2Ag alloy in the AC (a,c,e) and ST (b,d,f) conditions, at both low and high magnifications.

Moreover, the cross-sectional FESEM micrographs of both samples are presented in Figure 4. In general, it can be suggested that the coating formed on both samples is well bonded to the substrate, where no obvious microdefect was noticed in the substrate/coating interface. Furthermore, the average coating thickness of the Mg-2Ag alloy in the AC and ST states was measured to be about 71.1 and 142.6 μm, respectively, implying that in addition to a more uniform and dense coating, the heat-treated alloy possessed a thicker coating as well.

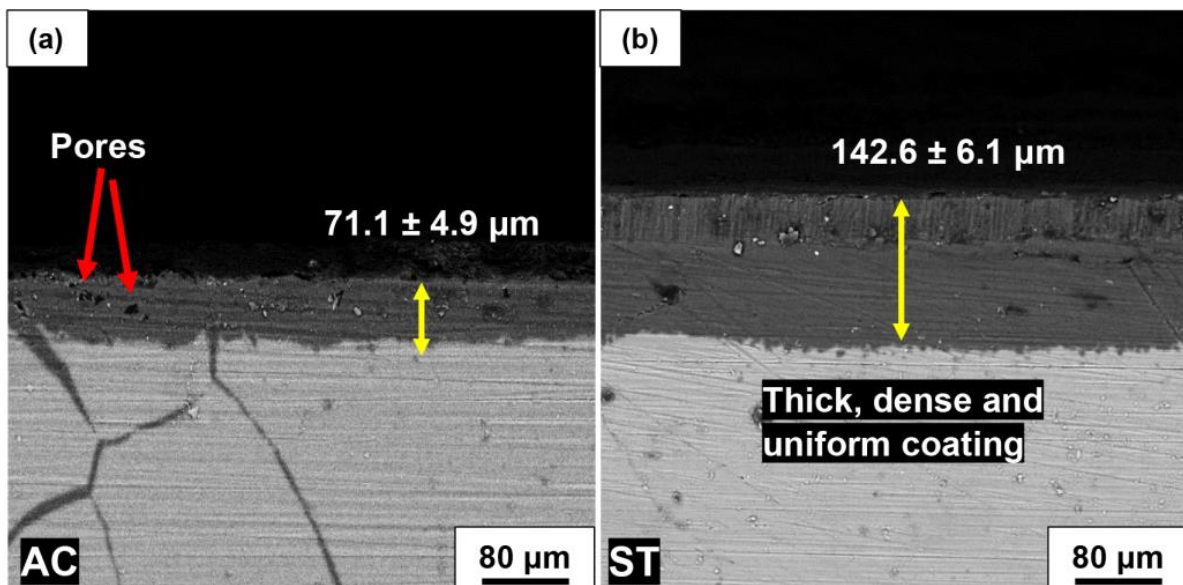


Figure 4. FESEM cross-sectional views of the coated Mg-2Ag alloy in the AC (a) and ST (b) states.

The microstructure of the substrate is believed to have a remarkable influence on the coating characteristics of biodegradable Mg alloys [37,45]. As was discussed and shown in Figures 1 and 2, the as-cast Mg-2Ag alloy exhibited a dendritic structure with silver segregation as well as $Mg_{54}Ag_{17}$ precipitates. Generally, coating nucleation would have different rates on different locations of a microstructure (e.g., α -Mg and Ag-rich precipitates). For instance, the nucleation rate on the secondary phases is significantly lower than the α -Mg, due to Mg deficiency on the secondary phases. This situation is exacerbated when the size of the precipitates is relatively large, which can make the $Mg(OH)_2$ nucleation and thickening extremely difficult. Such nonuniform rates of nucleation and growth in different regions of the substrate might lead to crack nucleation in the coating. Also, contracting stresses as a consequence of the drying stage in the hydrothermal coating process play an important role in crack generation in a loosely formed coating on Ag-rich secondary phases. In this regard, more defects in an as-cast Mg-2Ag coating can be attributed to its inhomogeneous microstructure with relatively large secondary phases. However, such problems were considerably mitigated by the implementation of heat treatment, where T4 treatment led to the approximately thorough dissolution of precipitates and uniformity of microstructure, and hence, improved quality of the coating. Modifying the microstructure and changing the size, morphology, and distribution of the secondary phases utilizing other postprocessing techniques like severe plastic deformation to enhance the hydrothermal coating quality of biodegradable Mg alloys has also been reported [14].

3.2. Corrosion Behavior

Figure 5 shows the corrosion results for the AC and ST materials in both the coated and coated conditions. Regarding the electrochemical test, the corrosion potential and corrosion current density values determined by the Tafel extrapolation are presented in Table 2. According to the polarization curves presented in Figure 5a, the solution-treated Mg-2Ag alloy exhibited decreased i_{corr} and nobler E_{corr} in comparison to the as-cast alloy. Furthermore, the coated alloys displayed significantly lower i_{corr} and more positive E_{corr} values, demonstrating the outstanding role of coating in improving the corrosion resistance of the Mg-2Ag alloy. Among the studied alloys, the coated solution-treated Mg-2Ag alloy manifested the best corrosion performance with the i_{corr} and E_{corr} of $1.84 \mu A/cm^2$ and $-0.26 V$, respectively.

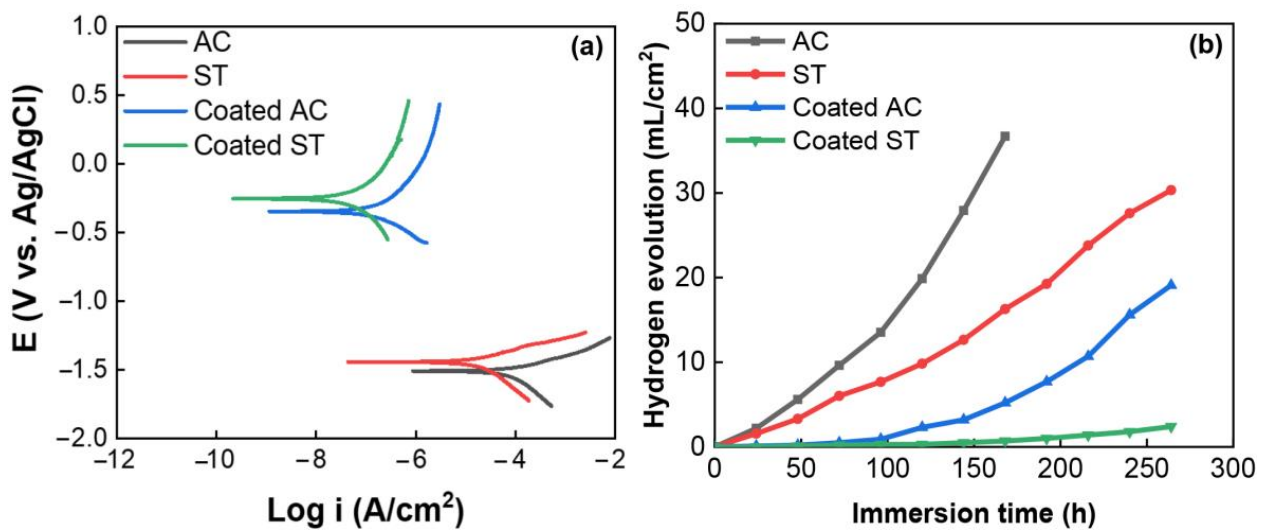


Figure 5. Polarization (a) and hydrogen evolution (b) curves of the uncoated and coated Mg-2Ag alloy in the AC and ST states.

Table 2. Summary of the electrochemical data of the studied alloys, acquired from polarization tests.

| Alloy | Condition | I_{corr} ($\mu\text{A}/\text{cm}^2$) | E_{corr} (V) | Corrosion Rate (mm/y) |
|---------------|-----------|--|----------------|---|
| Mg-2Ag | AC | 84.52 ± 2.4 | -1.52 | 1.93 ± 0.11 |
| | ST | 19.14 ± 1.6 | -1.44 | 0.44 ± 0.05 |
| Coated Mg-2Ag | AC | 4.12 ± 1.6 | -0.34 | 0.09 ± 0.01 |
| | ST | 1.84 ± 0.08 | -0.26 | 0.04 ± 0.01 |

Equation (1), a well-established equation in calculating the corrosion rate (mm/year) from the corrosion current density ($\mu\text{A}/\text{cm}^2$) [46], was used to determine the corrosion rates of the studied materials and the associated values are given in Table 2. Accordingly, it can be observed that solution heat treatment and hydrothermal coating can decrease the corrosion rate of the as-cast Mg-2Ag alloy from 1.93 to 0.04 mm/year .

$$\text{Corrosion rate} = 22.85 i_{corr} \quad (1)$$

The hydrogen evolution test was conducted for up to 242 h to assess the long-term degradability of alloys, and the corresponding results are plotted in Figure 5b. As can be noted, the volume of evolved hydrogen in the solution-treated Mg-2Ag alloy is considerably lower than the as-cast one. Video S1 shows the difference between the hydrogen gas evolution rate from the uncoated AC and coated ST samples. As can be noted in this video, while the uncoated AC alloy demonstrated the rapid production of hydrogen gas bubbles, the hydrogen bubbles can barely be observed on the surface of the coated ST sample. In addition, and in accordance with the polarization results, the line slope of the coated alloys, which is interpreted as the hydrogen evolution rate, is times lower than the uncoated alloys, indicating the notable protective impact of coating. It is interesting to note that there was no detectable volume of evolved hydrogen after the primary hours of immersion of the coated samples, implying the existence of an incubation period for these samples. These incubation periods were about 90 and 140 h for the coated AC and ST alloys, respectively. A longer incubation period implies greater protectiveness of the coating, since in fact, this period is proportional to the time required until the corrosive medium penetrates the coating and reaches the substrate.

Figure 6 illustrates the FESEM corrosion morphologies of the uncoated AC and coated ST samples (as the worst and best samples in terms of corrosion resistance, respectively),

after immersion in the PBS solution for 11 days. As can be observed, the uncoated as-cast alloy has been thoroughly corroded, where numerous cracks and deep pits, as well as stacked corrosion products, reside on its surface. In contrast, the coated ST alloy has only slightly changed after immersion in comparison with its morphology before immersion (Figure 3f), where a tightly integrated coating with few corrosion products is visible on its surface. Furthermore, whereas the FESEM cross-sectional micrograph of the coated ST alloy exhibits relatively no corrosion attacks, the uncoated AC one demonstrates severe and deep pitting (Figure 6c,d). As can be observed, the cross-sectional micrographs of the coated ST alloy before and after the degradation test show no or little changes, implying the efficiency of the applied coating and heat treatment in enhancing the degradation behavior of the Mg-2Ag alloy.

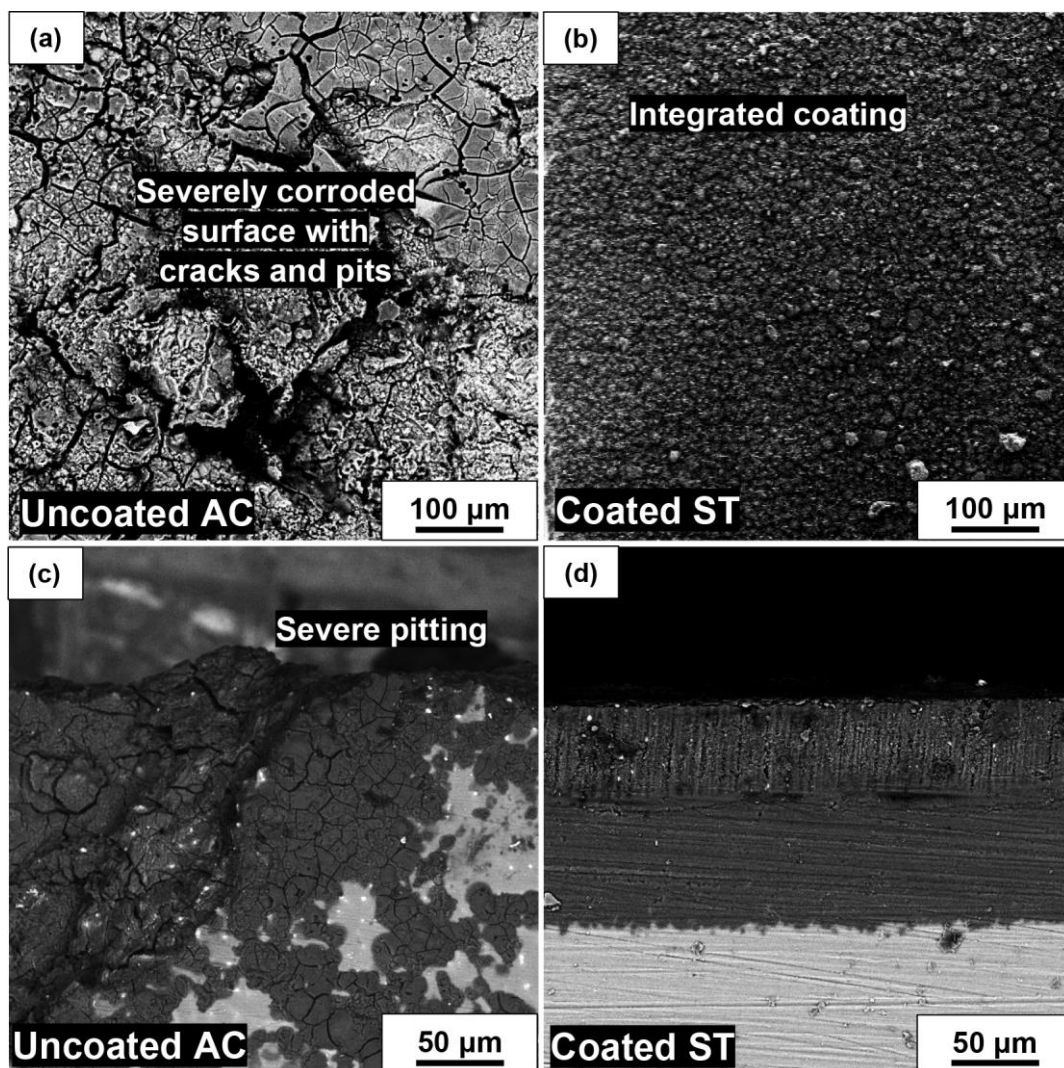


Figure 6. FESEM micrographs from surface (a,b) and cross-section (c,d) of the corroded samples after 11 days of immersion in the PBS solution. (a,c) Uncoated AC alloy, and (b,d) coated ST alloy.

It is generally believed that the dendritic microstructure of as-cast magnesium alloys with considerable alloying element segregation would significantly deteriorate the corrosion resistance [1]. Therefore, as indicated before, the high corrosion rate of the as-cast alloy can be attributed to the relatively large Ag-rich precipitates distributed inhomogeneously in the microstructure, resulting in pronounced microgalvanic corrosion. This phenomenon clearly appeared in Figure 6a as the deep pits and large cracks existing on the surface of the as-cast alloy. To address this issue, heat treatment has generally been employed and the

influence of this implementation has been comprehensively reviewed by the authors [1]. Also in this study, the solution treatment caused an almost complete dissolution of the precipitates, which would reduce the number of microgalvanic couples. Moreover, solution treatment can further affect the microstructure in terms of decreasing the casting defects and segregations, as well as internal stresses, leading to the enhanced corrosion resistance of the solution-treated Mg-2Ag alloy.

Coating provides a strong barrier between the substrate and corrosive medium, resulting in a significantly higher corrosion resistance of the coated samples. Such an effect is more substantial in the early stages of immersion, where the corrosive medium cannot reach the substrate, leading to a prolonged incubation period in the coated alloys. In this regard, there are two main parameters that play vital roles in the degradability of coated alloys: (1) the quality of the coating, and (2) the corrosion resistance of the substrate. Regarding the first parameter, and as long as the corrosive medium has not reached the substrate, a more integrated and compact coating would impede the infiltration of the PBS solution, while a porous coating with deep cracks can facilitate this process. Once the substrate surface is exposed to a corrosive solution, the corrosion resistance of the substrate becomes a governing parameter, where a lower degradation rate of the substrate can lead to an improved corrosion resistance of the coated alloy. In this regard, the superior corrosion performance of the coated solution-treated Mg-2Ag alloy can be ascribed to both the improved coating quality as well as higher substrate corrosion resistance. Figure 7 illustrates a schematic representation of the degradation behavior of the studied alloys.

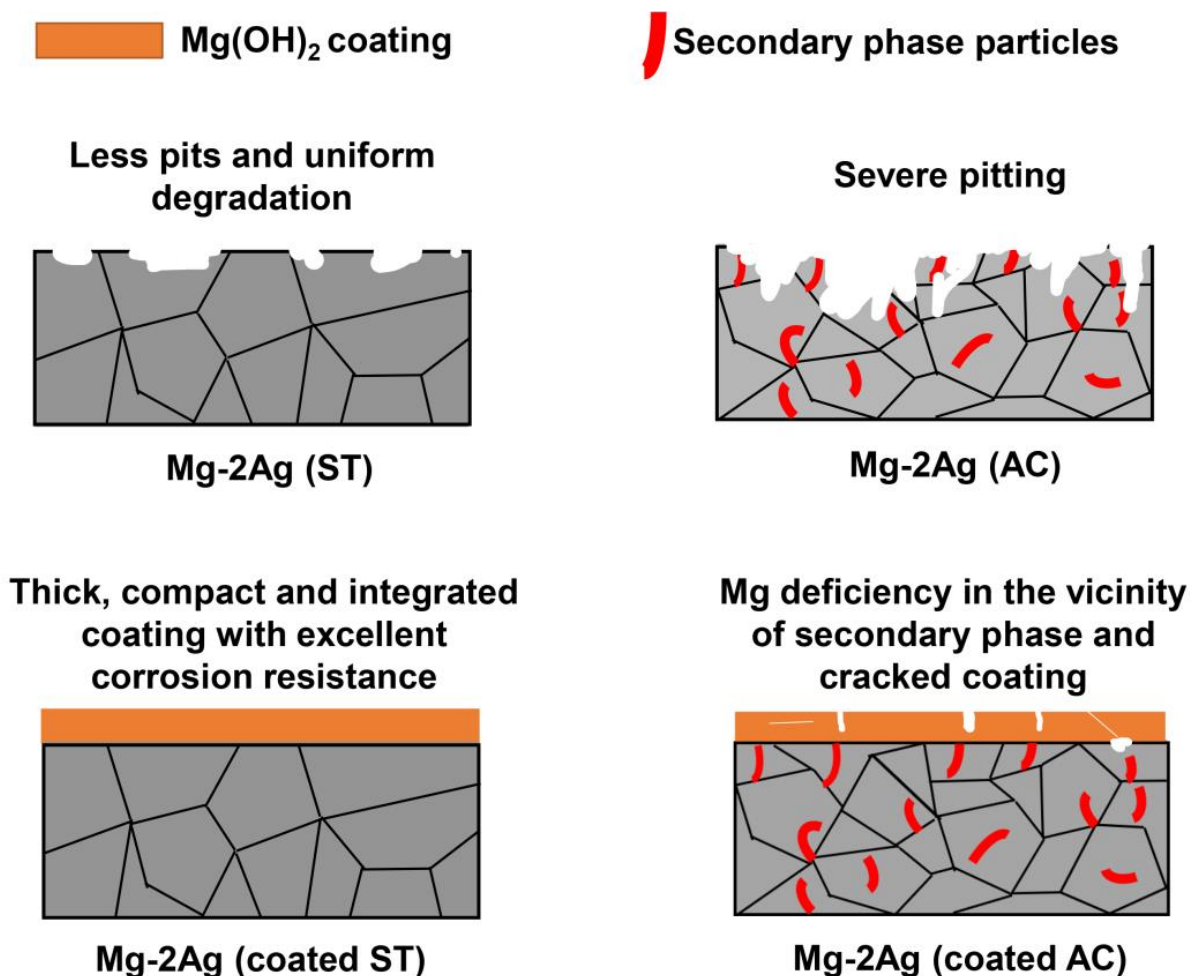


Figure 7. Schematic representation of degradation behavior of uncoated and coated Mg-2Ag alloy in the AC and ST states, reproduced from [14], with permission from Elsevier, 2022.

As was reported in our previous study [15], the addition of 2% Ag to the Mg matrix did not produce any sign of cytotoxicity, where cell viability and attachment were improved with the cell culture time. In addition, this alloy possessed sufficient antibacterial activity to prevent biofilm formation [43]. Thus, remarkably enhancing the corrosion resistance of the biodegradable Mg-2Ag alloy with a hydrothermal coating and solution treatment can be a great way of tackling its main challenges, and thus, introducing this alloy as a promising degradable implant.

4. Conclusions

The hydrothermal coating technique was employed to synthesize a protective coating on the biodegradable Mg-2Ag alloy using distilled water as the reagent. Coating was successfully formed on the alloy in both the as-cast and solution-treated conditions, which significantly enhanced the corrosion resistance in comparison with the uncoated ones. However, the coating characteristics and subsequent degradability were strongly dependent on the microstructure of the substrate, where the as-cast alloy with relatively large Ag-rich precipitates resulted in an inferior coating quality with many cracks and holes. In contrast, the dissolution of the secondary phases and homogenization of the microstructure with solution-treatment implementation noticeably improved the coating efficiency, and thus, the corrosion resistance. Overall, the hydrothermally coated solution-treated Mg-2Ag alloy shows promising results to be utilized as a biodegradable implant.

Supplementary Materials: The following supporting information can be downloaded at: <https://www.mdpi.com/article/10.3390/met13071260/s1>, Video S1: A video showing different rates of gas formation on the surface of uncoated AC and coated ST samples.

Author Contributions: M.M.-Z.: Conceptualization, investigation, writing—original draft, methodology, validation, formal analysis, writing—review and editing, visualization. M.Z.: investigation, methodology, formal analysis, writing—original draft. R.A.: supervision, conceptualization, writing—review and editing, project administration, funding acquisition. All authors have read and agreed to the published version of the manuscript.

Funding: This research received no external funding.

Data Availability Statement: The data presented in this study are available on request from the corresponding author.

Conflicts of Interest: The authors declare no conflict of interest.

References

1. Mohammadi Zerankeshi, M.; Alizadeh, R.; Gerashi, E.; Asadollahi, M.; Langdon, T.G. Effects of Heat Treatment on the Corrosion Behavior and Mechanical Properties of Biodegradable Mg Alloys. *J. Magnes. Alloys* **2022**, *10*, 1737–1785. [CrossRef]
2. Kumar, K.; Gill, R.S.; Batra, U. Challenges and Opportunities for Biodegradable Magnesium Alloy Implants. *Mater. Technol.* **2018**, *33*, 153–172. [CrossRef]
3. Nie, Y.J.; Dai, J.W.; Zhang, X.B. Effect of Ag Addition on Microstructure, Mechanical and Corrosion Properties of Mg–Nd–Zn–Zr Alloy for Orthopedic Application. *Acta Metall. Sin. (Engl. Lett.)* **2023**, *36*, 295–309. [CrossRef]
4. Lin, X.; Saijilafu; Wu, X.; Wu, K.; Chen, J.; Tan, L.; Witte, F.; Yang, H.; Mantovani, D.; Zhou, H.; et al. Biodegradable Mg-Based Alloys: Biological Implications and Restorative Opportunities. *Int. Mater. Rev.* **2022**, *68*, 365–403. [CrossRef]
5. Li, D.; Zhang, D.; Yuan, Q.; Liu, L.; Li, H.; Xiong, L.; Guo, X.; Yan, Y.; Yu, K.; Dai, Y.; et al. In Vitro and in Vivo Assessment of the Effect of Biodegradable Magnesium Alloys on Osteogenesis. *Acta Biomater.* **2022**, *141*, 454–465. [CrossRef]
6. Agarwal, S.; Curtin, J.; Duffy, B.; Jaiswal, S. Biodegradable Magnesium Alloys for Orthopaedic Applications: A Review on Corrosion, Biocompatibility and Surface Modifications. *Mater. Sci. Eng. C* **2016**, *68*, 948–963. [CrossRef]
7. Zhao, D.; Witte, F.; Lu, F.; Wang, J.; Li, J.; Qin, L. Current Status on Clinical Applications of Magnesium-Based Orthopaedic Implants: A Review from Clinical Translational Perspective. *Biomaterials* **2016**, *112*, 287–302. [CrossRef]
8. Zheng, Y.F.; Gu, X.N.; Witte, F. Biodegradable Metals. *Mater. Sci. Eng. R Rep.* **2014**, *77*, 1–34. [CrossRef]
9. Mohammadi-Zerankeshi, M.; Alizadeh, R. 3D-Printed PLA-Gr-Mg Composite Scaffolds for Bone Tissue Engineering Applications. *J. Mater. Res. Technol.* **2023**, *22*, 2440–2446. [CrossRef]
10. Sabbaghian, M.; Mahmudi, R.; Shin, K.S. Microstructure, Texture, Mechanical Properties and Biodegradability of Extruded Mg–4Zn–xMn Alloys. *Mater. Sci. Eng. A* **2020**, *792*, 139828. [CrossRef]

11. Chen, J.; Tan, L.; Yang, K. Recent Advances on the Development of Biodegradable Magnesium Alloys: A Review. *Mater. Technol.* **2016**, *31*, 681–688. [[CrossRef](#)]
12. Liu, D.; Yang, D.; Li, X.; Hu, S. Mechanical Properties, Corrosion Resistance and Biocompatibilities of Degradable Mg-RE Alloys: A Review. *J. Mater. Res. Technol.* **2019**, *8*, 1538–1549. [[CrossRef](#)]
13. Mohammadi Zerankeshi, M.; Alizadeh, R. Ag-Incorporated Biodegradable Mg Alloys. *Materialia* **2022**, *23*, 101445. [[CrossRef](#)]
14. Zohrevand, M.; Mohammadi-Zerankeshi, M.; Nobakht-Farin, F.; Alizadeh, R.; Mahmudi, R. Degradation Behavior of the As-Extruded and ECAP-Processed Mg-4Zn Alloy by Ca Addition and Hydrothermal Coating. *J. Mater. Res. Technol.* **2022**, *20*, 1204–1215. [[CrossRef](#)]
15. Mohammadi-Zerankeshi, M.; Alizadeh, R.; Labbaf, S. Improving Mechanical, Degradation and Biological Behavior of Biodegradable Mg-2Ag Alloy: Effects of Y Addition and Heat Treatment. *J. Mater. Res. Technol.* **2023**, *22*, 1677–1694. [[CrossRef](#)]
16. Gao, Y.; Zhao, P.; Cao, X.Q.; Misra, R.D.K.; Wang, W.; Chen, K.Z. Tin-Induced Microstructural Changes and Associated Corrosion Resistance of Biodegradable Mg-Zn Alloy. *Rare Met.* **2022**, *41*, 883–888. [[CrossRef](#)]
17. Zhang, Y.; Feng, X.; Huang, Q.; Li, Y.; Yang, Y. Enhancing Mechanical Properties and Degradation Performance of Mg-0.8wt.%Ca Alloy by Directional Solidification. *Trans. Nonferrous Met. Soc. China* **2023**, *33*, 409–421. [[CrossRef](#)]
18. Chernousova, S.; Eppler, M. Silver as Antibacterial Agent: Ion, Nanoparticle, and Metal. *Angew. Chem. Int. Ed.* **2013**, *52*, 1636–1653. [[CrossRef](#)]
19. Liu, Z.; Schade, R.; Luthringer, B.; Hort, N.; Rothe, H.; Müller, S.; Liefeth, K.; Willumeit-Römer, R.; Feyerabend, F. Influence of the Microstructure and Silver Content on Degradation, Cytocompatibility, and Antibacterial Properties of Magnesium-Silver Alloys in Vitro. *Oxid. Med. Cell. Longev.* **2017**, *2017*, 8091265. [[CrossRef](#)] [[PubMed](#)]
20. Applications, O.; Dai, Y.; Liu, H.; Tang, Y.; Xu, X.; Long, H.; Yan, Y. A Potential Biodegradable Mg-Y-Ag Implant with Strengthened Antimicrobial Properties in Orthopedic Applications. *Metals* **2018**, *8*, 948. [[CrossRef](#)]
21. Bian, M.; Huang, X.; Chino, Y. A Combined Experimental and Numerical Study on Room Temperature Formable Magnesium e Silver e Calcium Alloys. *J. Alloys Compd.* **2020**, *834*, 155017. [[CrossRef](#)]
22. Lu, Y.; Bradshaw, A.R.; Chiu, Y.L.; Jones, I.P. Effects of Secondary Phase and Grain Size on the Corrosion of Biodegradable—Zn—Ca Alloys. *Mater. Sci. Eng. C* **2015**, *48*, 480–486. [[CrossRef](#)]
23. Janbozorgi, M.; Karimi Taheri, K.; Karimi Taheri, A. Microstructural Evolution, Mechanical Properties, and Corrosion Resistance of a Heat-Treated Mg Alloy for the Bio-Medical Application. *J. Magnes. Alloys* **2019**, *7*, 80–89. [[CrossRef](#)]
24. Bryła, K.; Horky, J.; Krystian, M.; Lityńska-Dobrzyńska, L.; Mingler, B. Microstructure, Mechanical Properties, and Degradation of Mg-Ag Alloy after Equal-Channel Angular Pressing. *Mater. Sci. Eng. C* **2020**, *109*, 110543. [[CrossRef](#)] [[PubMed](#)]
25. Yin, Z.Z.; Qi, W.C.; Zeng, R.C.; Chen, X.B.; Gu, C.D.; Guan, S.K.; Zheng, Y.F. Advances in Coatings on Biodegradable Magnesium Alloys. *J. Magnes. Alloys* **2020**, *8*, 42–65. [[CrossRef](#)]
26. Zheng, T.; Hu, Y.; Zhang, Y.; Pan, F. Formation of a Hydrophobic and Corrosion Resistant Coating on Magnesium Alloy via a One-Step Hydrothermal Method. *J. Colloid Interface Sci.* **2017**, *505*, 87–95. [[CrossRef](#)] [[PubMed](#)]
27. Zhao, C.; Wu, H.; Hou, P.; Ni, J.; Han, P.; Zhang, X. Enhanced Corrosion Resistance and Antibacterial Property of Zn Doped DCPD Coating on Biodegradable Mg. *Mater. Lett.* **2016**, *180*, 42–46. [[CrossRef](#)]
28. Yamauchi, N.; Ueda, N.; Okamoto, A.; Sone, T.; Tsujikawa, M.; Oki, S. DLC Coating on Mg-Li Alloy. *Surf. Coat. Technol.* **2007**, *201*, 4913–4918. [[CrossRef](#)]
29. Gao, Y.L.; Liu, Y.; Song, X.Y. Plasma-Sprayed Hydroxyapatite Coating for Improved Corrosion Resistance and Bioactivity of Magnesium Alloy. *J. Therm. Spray Technol.* **2018**, *27*, 1381–1387. [[CrossRef](#)]
30. Minting, D.; Linlin, H.; Mengke, P.; Fenyang, H.; Qiang, G.; Yashao, C.; Peng, L. Preparation of Vancomycin-Loaded Alginate Hydrogel Coating on Magnesium Alloy with Enhanced Anticorrosion and Antibacterial Properties. *Thin Solid Films* **2020**, *693*, 137679. [[CrossRef](#)]
31. Chang, L.; Wang, P.; Liu, W. Effect of Amino Acids on the Structure and Corrosion Resistance of Mg-Li Alloy Anodic Oxide Film. *Adv. Mater. Res.* **2011**, *146–147*, 785–788. [[CrossRef](#)]
32. Zhang, B.; Yao, R.; Li, L.; Wang, Y.; Luo, R.; Yang, L.; Wang, Y. Green Tea Polyphenol Induced Mg²⁺-Rich Multilayer Conversion Coating: Toward Enhanced Corrosion Resistance and Promoted In Situ Endothelialization of AZ31 for Potential Cardiovascular Applications. *ACS Appl. Mater. Interfaces* **2019**, *11*, 41165–41177. [[CrossRef](#)]
33. Zhang, L.; Xu, M.; Hu, Y.; Gao, F.; Gong, T.; Liu, T.; Li, X.; Pan, C. Biofunctionalization of Biodegradable Magnesium Alloy to Improve the In Vitro Corrosion Resistance and Biocompatibility. *Appl. Surf. Sci.* **2018**, *451*, 20–31. [[CrossRef](#)]
34. Gao, F.; Hu, Y.; Li, G.; Liu, S.; Quan, L.; Yang, Z.; Wei, Y.; Pan, C. Bioactive Materials Layer-by-Layer Deposition of Bioactive Layers on Magnesium Alloy Stent Materials to Improve Corrosion Resistance and Biocompatibility. *Bioact. Mater.* **2020**, *5*, 611–623. [[CrossRef](#)] [[PubMed](#)]
35. Gupta, R.K.; Mensah-Darkwa, K.; Kumar, D. Corrosion Protective Conversion Coatings on Magnesium Disks Using a Hydrothermal Technique. *J. Mater. Sci. Technol.* **2014**, *30*, 47–53. [[CrossRef](#)]
36. Song, D.; Lian, B.; Fu, Y.; Wang, G.; Qiao, Y.; Klu, E.E.; Gong, X.; Jiang, J. Dual-Layer Corrosion-Resistant Conversion Coatings on Mg-9li Alloy via Hydrothermal Synthesis in Deionized Water. *Metals* **2021**, *11*, 1396. [[CrossRef](#)]
37. Song, D.; Guo, G.; Jiang, J.; Zhang, L.; Ma, A.; Ma, X.; Chen, J.; Cheng, Z. Hydrothermal Synthesis and Corrosion Behavior of the Protective Coating on Mg-2Zn-Mn-Ca-Ce Alloy. *Prog. Nat. Sci. Mater. Int.* **2016**, *26*, 590–599. [[CrossRef](#)]

38. Song, D.; Li, C.; Zhang, L.; Ma, X.; Guo, G.; Zhang, F.; Jiang, J.; Ma, A. Decreasing Bio-Degradation Rate of the Hydrothermal-Synthesizing Coated Mg Alloy via Pre-Solid-Solution Treatment. *Materials* **2017**, *10*, 858. [[CrossRef](#)] [[PubMed](#)]
39. Wang, Z.; Su, Y.; Li, Q.; Liu, Y.; She, Z.; Chen, F.; Li, L.; Zhang, X.; Zhang, P. Researching a Highly Anti-Corrosion Superhydrophobic Film Fabricated on AZ91D Magnesium Alloy and Its Anti-Bacteria Adhesion Effect. *Mater. Charact.* **2015**, *99*, 200–209. [[CrossRef](#)]
40. Jiang, D.; Li, Q.K.; Liu, Y.Z.; Xiao, Z.; Xia, B.H.; Li, S.Q.; Zhang, F.; Cui, L.Y.; Zeng, R.C. Polyphosphate Assisted Hydrothermal Synthesis of Hydroxyapatite Coating on Mg Alloys: Enhanced Mechanical Properties and Corrosion Resistance. *Surf. Coat. Technol.* **2022**, *432*, 128033. [[CrossRef](#)]
41. Ling, L.; Cai, S.; Li, Q.; Sun, J.; Bao, X.; Xu, G. Recent Advances in Hydrothermal Modification of Calcium Phosphorus Coating on Magnesium Alloy. *J. Magnes. Alloys* **2021**, *10*, 62–80. [[CrossRef](#)]
42. Zhu, Y.; Wu, G.; Zhang, Y.; Zhao, Q. Applied Surface Science Growth and Characterization of Mg(OH)₂ Film on Magnesium Alloy AZ31. *Appl. Surf. Sci.* **2011**, *257*, 6129–6137. [[CrossRef](#)]
43. Tie, D.; Feyerabend, F.; Müller, W.; Schade, R.; Liefelth, K.; Kainer, K.; Willumeit, R. Antibacterial Biodegradable Mg-Ag Alloys. *Eur. Cell. Mater.* **2013**, *25*, 284–298, discussion 298. [[CrossRef](#)] [[PubMed](#)]
44. Zhu, Y.; Zhao, Q.; Zhang, Y.H.; Wu, G. Hydrothermal Synthesis of Protective Coating on Magnesium Alloy Using De-Ionized Water. *Surf. Coat. Technol.* **2012**, *206*, 2961–2966. [[CrossRef](#)]
45. Song, D.; Li, C.; Liang, N.; Yang, F.; Jiang, J.; Sun, J.; Wu, G.; Ma, A.; Ma, X. Simultaneously Improving Corrosion Resistance and Mechanical Properties of a Magnesium Alloy via Equal-Channel Angular Pressing and Post Water Annealing. *Mater. Des.* **2019**, *166*, 107621. [[CrossRef](#)]
46. Jiang, D.; Dai, Y.; Zhang, Y.; Yan, Y.; Ma, J.; Li, D.; Yu, K. Effects of Heat Treatment on Microstructure, Mechanical Properties, Corrosion Resistance and Cytotoxicity of ZM21 Magnesium Alloy as Biomaterials. *J. Mater. Eng. Perform.* **2019**, *28*, 33–43. [[CrossRef](#)]

Disclaimer/Publisher's Note: The statements, opinions and data contained in all publications are solely those of the individual author(s) and contributor(s) and not of MDPI and/or the editor(s). MDPI and/or the editor(s) disclaim responsibility for any injury to people or property resulting from any ideas, methods, instructions or products referred to in the content.